Available online at www.sciencedirect.com
SCIENCE DIRECT
Journal of Colloid and Interface Science 285 (2005) 609–618
JOURNAL OF Colloid and Interface Science
www.elsevier.com/locate/jcis

Electrostatic potential around charged finite rodlike macromolecules: nonlinear Poisson–Boltzmann theory

David Chapot [a], Lydéric Bocquet [b,*], Emmanuel Trizac [c]

[a] *Laboratoire de Physique de l'E.N.S. de Lyon, UMR CNRS 5672, 46 Allée d'Italie, 69364 Lyon Cedex, France*
[b] *Laboratoire de Physique de Matière Condensée et Nanostructures, Université Lyon 1, 69622 Villeurbanne Cedex, France*
[c] *Laboratoire de Physique Théorique et Modèles Statistiques, UMR CNRS 8626, Université Paris-Sud, 91405 Orsay Cedex, France*

Received 21 July 2004; accepted 29 November 2004

Available online 27 January 2005

Abstract

In this paper, we show that the far field electrostatic potential created by a *highly charged* finite size cylinder within the nonlinear Poisson–Boltzmann (PB) theory, is remarkably close to the potential created within the linearized PB approximation by the same object at a well-chosen fixed potential. Comparing the nonlinear electrostatic potential with its linear counterpart associated to a fixed potential boundary condition (called the effective surface potential), we deduce the effective charge of the highly charged cylinder. Values of the effective surface potential are provided as a function of the bare surface charge and Debye length of the ionic solution. This allows to compute the anisotropic electrostatic interaction energy of two distant finite rods.

Keywords: Nonlinear Poisson–Boltzmann theory; Linear Poisson–Boltzmann theory; Charged finite rods; Effective surface potential; Effective charge; Electrostatic interaction energy

1. Introduction

Electrostatic interactions between charged macromolecules play a key role in the understanding of the structure and phase behavior of polyelectrolytes or colloidal suspensions. Interaction between charged colloids in a ionic medium are generally described within the framework of DLVO theory, named after Derjaguin, Landau, Verwey, and Overbeek [10]. The interaction energy between two spherical colloids with charge Ze and identical radius a takes the form of the so-called DLVO potential,

$$U_{12}(r) = \frac{Z^2 e^2}{4\pi\epsilon}\left(\frac{\exp[\kappa_D a]}{1+\kappa_D a}\right)^2 \frac{\exp(-\kappa_D r)}{r}, \tag{1}$$

where e is the elementary charge and κ_D denotes the inverse Debye screening length. The latter is defined in terms of the micro-ions bulk densities $\{\rho_\alpha\}$ (with valencies $\{z_\alpha\}$) as $\kappa_D^2 = 4\pi\ell_B\sum_\alpha \rho_\alpha z_\alpha^2$. The solvent is described at the level of a dielectric continuum approximation with permittivity ϵ, and the Bjerrum length ℓ_B is defined as $\ell_B = e^2/(4\pi\epsilon k_B T)$, where $k_B T$ is the thermal energy.

However, the spherical shape is not the rule in nature and colloids often take the form of anisotropic particles. Examples are numerous, such as clay platelets (laponite, montmorillonite, gibbsite) [1–3], ribbons (vanadium pentoxide V_2O_5) [4], rigid rods (Tobacco Mosaïc Virus—TMV, boehmite, goethite) [5,6], to cite a few. Due to their anisotropy these systems may exhibit orientational order (nematic, smectic, etc.) or may even organize into supramolecular structures like multiple helixes or lamellar multilayers [7,8]. From the theoretical point of view, Onsager in a pioneering work has provided the first description of the entropy driven isotropic-to-nematic (I–N) transition [9] in an assembly of (infinitely long) rods. In the case of charged polyelectrolytes, the results for the uncharged rods might be extended using the intuitive concept of "dressed" rods, which amounts to increasing the bare radius of the

* Corresponding author.
E-mail address: lbocquet@lpmcn.univ-lyon1.fr (L. Bocquet).

0021-9797/$ – see front matter © 2005 Published by Elsevier Inc.
doi:10.1016/j.jcis.2004.11.059

rod by the Debye length, the characteristic range of the screened Coulomb interaction. Stroobants and Lekkerkerker have provided a consistent description of this effect at the level of a second-virial-coefficient approximation [12]. Such an approach provides predictions in good agreement with the experimental observations, in particular for the volume fraction corresponding to the I–N transition of highly asymmetrical rodlike particles like the fd virus (ratio of height over radius $L/R = 250$) [11]. However the case of smaller aspect ratio is less clear cut. In particular, the dressed rod picture overestimates the I–N volume fraction for shorter rods like goethite ($L/R = 12$), even within more sophisticated versions of the dressed model [13,14]. Moreover, it is quite interesting to note that anisotropic charged colloids with intermediate aspect ratio exhibit quite systematically "gel" phases, competing with the orientational transitions, which are not predicted by theoretical approaches based on an isotropic Yukawa interaction [15]. This is, e.g., the case for laponite (disks) and boehmite (rods) [3,16–22,24]. The origin and nature of these transitions—experimentally debated [26,27]—which occur at small volume fractions are still unclear today.

Coming back to basic ingredients, the electrostatic interaction between moderately anisotropic colloids should therefore be specifically reconsidered. In a recent paper [23], we have generalized the DLVO description to express the interaction between charged colloids of arbitrary shapes (such as disks or rods). This framework provides a general expression of the interaction between two colloids, which has the same status as the DLVO potential, now for arbitrary shapes. It turns out that the interactions remain anisotropic at all distances (see also [24,28]).

However, beyond these results, the calculations in [23] rely on two specific assumption: (i) micro-ions are described at the level of the *linearized Poisson–Boltzmann* (LPB) approximation; (ii) colloids are assumed to be characterized by a *constant surface potential*. Note that these are the assumptions underlying the expression of the DLVO interaction potential, Eq. (1) [10]. In this paper, we reconsider the validity of this approach to compute the interaction between two charged colloids. In particular, we will show that these assumptions are justified for finite rod-like polyelectrolytes within the nonlinear Poisson–Boltzmann (NLPB) description, in the saturation limit where the bare charge of the colloid is *large*. More precisely, we will show that the electrostatic potential created by a strongly charged (anisotropic) colloid computed at the NLPB level coincides with the electrostatic potential of a colloid with a fixed surface potential, called the effective surface potential, computed at LPB level. This result is valid for large distances from the colloid, corresponding to the "far-field" limit.

In a previous work [25], we have shown that this identification naturally emerges in the case of charged spherical colloids or infinite rods, and can be justified on the basis of an asymptotic matching procedure in the case where the Debye length is smaller than the radius a of the colloid, i.e., $\kappa_D a \gg 1$ [29]. A simple physical picture of this effect is that micro-ions strongly accumulate in the vicinity of the colloid surface for a sufficiently large bare charge, resulting in a strong screening of the electrostatic potential in the first few micro-ion layers close to the surface. In other words, the interaction at large distance is not characterized by the bare charge, but by an effective, much lower one. For spherical and cylinder like shapes, this effective charge is fixed at the LPB level from the effective condition of a fixed potential, Φ_0, on the surface of the colloid. This condition is independent of the bare charge of the colloid provided it is sufficiently large (saturation limit). Moreover in the $\kappa_D a \gg 1$ limit, Φ_0 reduces simply to $\Phi_0 = 4k_B T/e$.

This paper is organized into two parts:

- In a first part, we solve the NLPB equation for finite-size rod-like polyelectrolytes, with prescribed surface charge density.
- In a second part, we compare these NLPB results for the electrostatic potential, with the predictions of the *linearized* Poisson–Boltzmann equation, associated with a fixed potential on the surface of the cylinder.

All results will be written in terms of dimensionless variables. All the lengths (such as ℓ_B, κ_D^{-1}, or L) are expressed in terms of the radius of the cylinder R: $L^{\text{adim}} = L/R$, $\kappa_D^{\text{adim}} = \kappa_D R$, etc. Dimensionless electrostatic potential Φ and surface charge densities are defined respectively as $\Phi^{\text{adim}} = e\Phi/k_B T$ and $\sigma^{\text{adim}} = 4\pi\ell_B R\sigma/e$, where ℓ_B is the Bjerrum length defined by $\ell_B = e^2/(4\pi\varepsilon k_B T)$ (for water at room temperature, $\ell_B = 7$ Å). From now on, the index adim will be skipped, but we will keep $R = 1$ in the formulas to allow the reader to recover the initial dimensions.

2. Calculation of the NLPB electrostatic potential for finite size objects

2.1. Method of resolution of NLPB in a Wigner–Seitz cell

We consider a cylinder, immersed in a monovalent liquid medium with Debye length ℓ_D and carrying a given surface charge density σ. The NLPB equation reads

$$\Delta\Phi = \kappa_D^2 \sinh\Phi, \tag{2}$$

and the boundary conditions are written (in dimensionless form)

$$\sigma = -\frac{\partial\Phi}{\partial\mathbf{n}}, \tag{3}$$

where $\mathbf{n}$ is the outer unitary vector perpendicular to the surface of the colloid. To solve Eq. (2), we make use of a Wigner–Seitz cell and use a procedure introduced in [30]. The colloids are assumed to be confined into cylindrical cells of volume V. The normal component of the electrical field $\mathbf{E}$ vanishes on the surface of the WS cell. We denote the radius

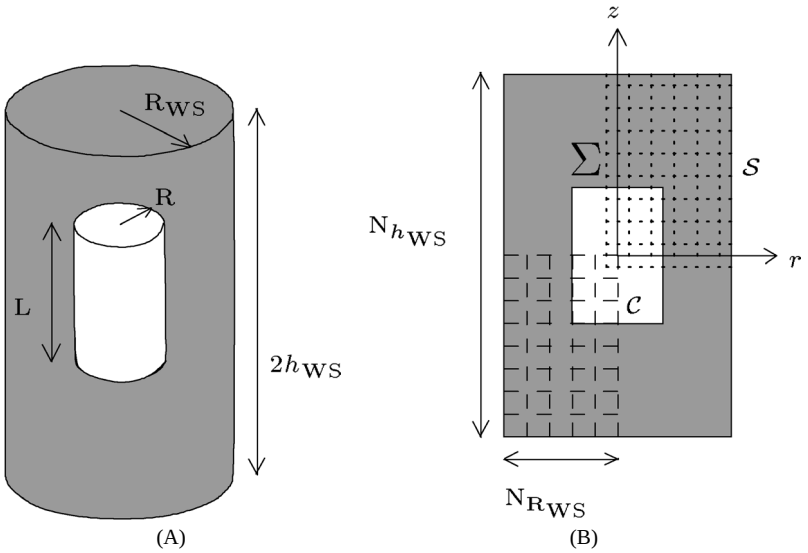

Fig. 1. The Wigner–Seitz cell. In A, the finite cylinder $\mathcal{C}$ of radius R and length L and the WS cell of radius R_{WS} and height h_{WS} are represented in perspective. In the lower left part of B the lattice of $N_{R_{\mathrm{WS}}} \times N_{h_{\mathrm{WS}}}/2$ points used to represent the electrostatic potential has been plotted with dashed lines. The upper right part of B shows with dotted lines the cells used to compute integrals in the WS cell, which surrounds the points on the previously defined WS (dual) lattice.

and height of the WS cell as R_{WS} and h_{WS}, as represented on Fig. 1, such that $\pi R_{\mathrm{WS}}^2 h_{\mathrm{WS}} = V$. In the present paper, we are mostly interested in the infinite dilution limit of one isolated cylinder in the liquid medium. The WS cell, which is used for technical convenience, needs therefore be large enough (characteristic dimensions much larger than the Debye length).

To solve the NLPB equation in the WS geometry, the NLPB equation is rewritten as a self consistent equation, by transforming it from the action of a *linear* operator applied to the potential Φ, with sources composed of the charge carried by the cylinder and of a nonlinear term depending on Φ [30]. The solution is then obtained by solving this self-consistent equation iteratively, using the Green function formalism. The details have been gathered in Appendix A.

2.2. Benchmark results for the NLPB electrostatic potential

Before addressing the problem of a rod-like polyelectrolyte, we first consider two benchmark geometries, in order to test the numerical procedure described in Appendices A and B. The potential obtained from this procedure is denoted Φ_{nl}.

The first case is that of an infinite charged plane, which is exactly obtained within our geometry when $R_{\mathrm{WS}} = R$ and $h_{\mathrm{WS}} \gg L/2$. The "colloid" then takes the form of a planar slab. The NLPB equation can be exactly solved for this geometry (see, e.g., [25]) and is compared in Fig. 2 with the numerical solution obtained within the present approach. Note that the potential inside the slab is expected to be constant. In the numerical calculations, different grids have been tested, showing that outside the colloid, the numerical solution converges quite fast to the exact solution, even for loose discretization grids. A good agreement is obtained outside

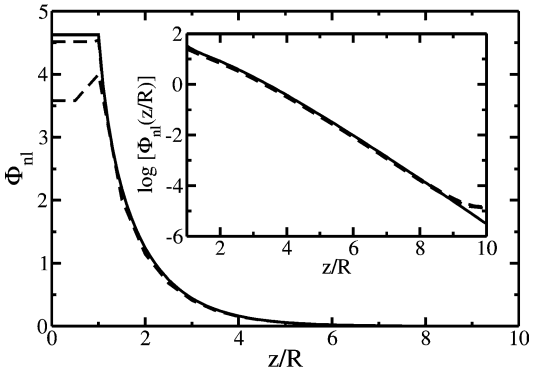

Fig. 2. Calculation of $\Phi_{\text{infinite plane}}$ for $\sigma = 10$ with different accuracies (dashed line) and comparison with the exact solution (continuous line). The parameters are the following: $R_{\mathrm{WS}} = R$, $N_{R_{\mathrm{WS}}} = 1$, $h_{\mathrm{WS}} = 10R$, $N_{h_{\mathrm{WS}}} = 40$ or 200. Although Φ_{nl} computed with 40 points along the z axis is obviously not constant inside the planar slab, it is in agreement with the exact solution outside. Note that the planar slab extends up to $z/R = 1$ in the present geometry.

the colloid, even if *inside* the solution has still not fully converged toward the exact $\Phi = \mathrm{cst}$ condition due to the discrete grid.

The same conclusions are reached for the other benchmark case, the infinite cylinder, which corresponds in our geometry to $R_{\mathrm{WS}} < R$ and $h_{\mathrm{WS}} = L/2$; see Fig. 3. The exact solution is found in this case using a numerical equation solver.

2.3. NLPB electrostatic potential around a rodlike polyelectrolyte

The two limiting cases presented in the previous section validate the numerical procedure used, which we now apply to rod-like polyelectrolytes with finite length. Figs. 4 and 5

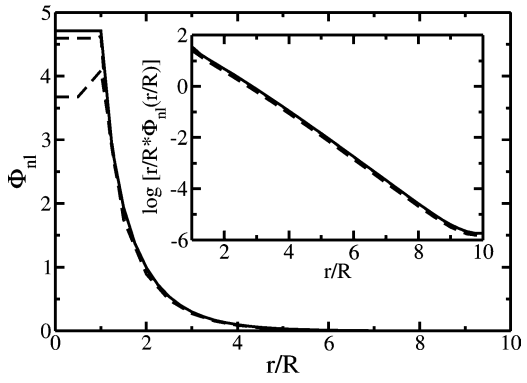

Fig. 3. Calculation of $\Phi_{\text{infinite cylinder}}$ for $\sigma = 12$ with different accuracies (dashed lines) and comparison with the exact solution (continuous line). The parameters are the following: $R_{\text{WS}} = 10R$, $N_{R_{\text{WS}}} = 20$ or 100, $h_{\text{WS}} = R$, $N_{h_{\text{WS}}} = 2$. Although Φ_{nl} computed with 20 points along the r axis is obviously not constant inside the cylinder, it is in agreement with the exact solution outside. Note that the WS cell imposes a vanishing derivative of the potential at $r/R = 10$. A similar phenomenon may be observed with the dashed line in the inset of Fig. 2 (the continuous line is free of such an effect since it corresponds to the result when $h_{\text{WS}} \to \infty$).

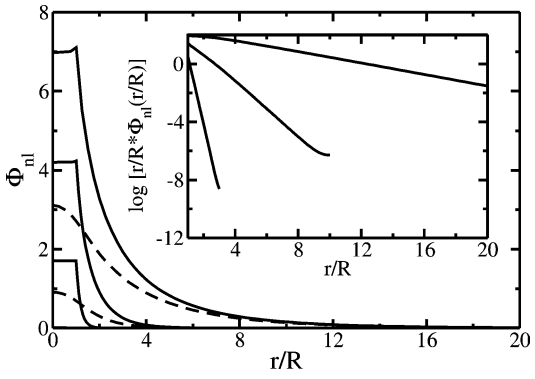

Fig. 4. Solution of the nonlinear PB equation Φ_{nl} in the plane $z = 0$ (continuous line) and $z = 3$ (dashed line) for $L/R = 4$, $\sigma = 10$, and $\kappa_{\text{D}}R = 0.2$, 1.0, and 5.0 (from top to bottom). On the vertical axis, the curves have been multiplied by an arbitrary factor for the sake of readability. The inset shows that Φ_{nl} decreases as $\exp(-\kappa_{\text{D}}r)/r$ in the plane $z = 0$.

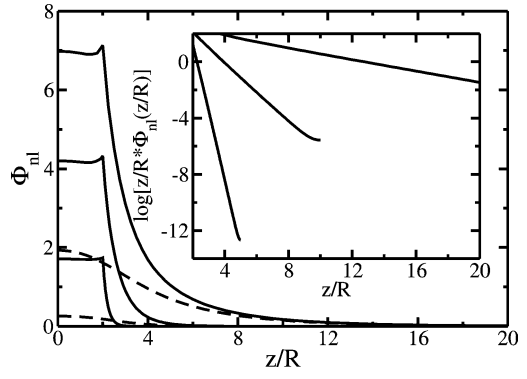

Fig. 5. Solution of the nonlinear PB equation Φ_{nl}, on the axis $r = 0$ (continuous line) and $r = 3$ (dashed line) for $L/R = 4$, $\sigma = 10$, and $\kappa_{\text{D}}R = 0.2$, 1.0, 5.0 from top to bottom. On the vertical axis, the curves have been multiplied by an arbitrary factor for the sake of readability. The inset shows that Φ_{nl} decreases as $\exp(-\kappa_{\text{D}}z)/z$ on the axis $r = 0$.

show typical results for the nonlinear potential created by a cylinder with a finite aspect ratio, here $L/R = 4$, immersed in an ionic liquid characterized by different Debye lengths (here $\kappa_{\text{D}}R = 0.2$, 0.5, or 1.0). As for the benchmark cases, the electrostatic potential *inside* the colloid is not exactly constant due to the discretization grid, but we have checked that the electrostatic potential *outside* the colloid becomes independent of the discretization step for the grids used.

3. Far-field behavior of the electrostatic potential

Having in mind the calculation *in fine* of electrostatic interactions between polyelectrolytes, our aim is now to extract the asymptotic behavior of the electrostatic potential from the numerical solution of the NLPB equation.

3.1. Asymptotic matching of the LPB and NLPB solution in the far field limit

At large distances from the colloid, i.e., distances typically larger than the Debye length, the electrostatic potential becomes small and the NLPB equation, Eq. (2), reduces therefore to the *linearized* Poisson–Boltzmann equation (LPB),

$$\Delta\Phi_{\text{lin}} = \kappa_{\text{D}}^2\Phi_{\text{lin}}. \tag{4}$$

To avoid confusion, we denote Φ_{lin} the solution of the LPB equation. This equation is much simpler than its nonlinear counterpart and can be solved using the Green function formalism; see, e.g., Ref. [23]. However, the main problem which still subsists concerns the *effective boundary conditions* which the LPB potential, Φ_{lin}, has to obey at the colloid surface, in order to match the solution, Φ_{nl}, of the NLPB equation in the asymptotic regime (distances larger than κ_{D}^{-1}).

In a previous work [25], it was shown that provided $\kappa_{\text{D}}R$ is large enough, this *effective boundary condition* reduces to a *fixed potential* at the surface of the colloid, in the saturation limit where the bare charge of the colloid is large. Two geometries were specifically considered in [25]: the sphere and the infinite cylinder. We show in the following that this condition also emerges in the case of anisotropic polyelectrolytes with finite aspect ratio. The solution of the LPB equation, Eq. (4), with a fixed surface potential boundary condition on the polyelectrolyte surface,

$$\Phi_{\text{lin}} = \Phi_0, \tag{5}$$

is discussed in Ref. [23] and we refer to this paper for technical details.

3.2. Numerical results

In this paragraph, we compare the solution of the NLPB equation (2) with a *fixed bare charge* boundary condition to

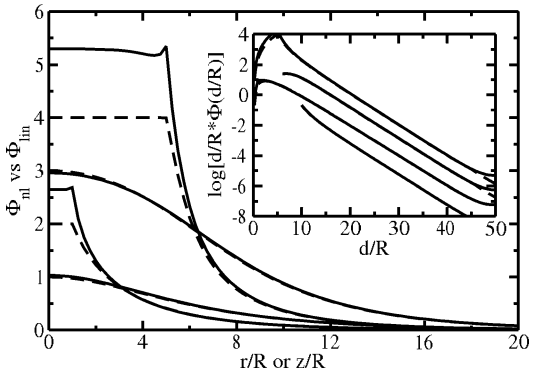

Fig. 6. Comparison between the solution of the NLPB equation with fixed bare charge boundary condition, $\Phi_{\rm nl}$ (solid line), and the solution, $\Phi_{\rm lin}$, of the LPB equation with a fixed effective surface potential boundary condition $\Phi_{\rm eff} = 5.41$ (dashed line). The aspect ratio is $L/R = 10$, the Debye length is $\kappa_{\rm D} R = 0.2$ and the bare charge is $\sigma = 10$. From top to bottom, the potential is computed on the axis $r = 0$, $r = R + \kappa_{\rm D}^{-1} = 6R$, $z = 0$, and $z = L/2 + \kappa_{\rm D}^{-1} = 10R$. On the vertical axis, the curves have been multiplied by an arbitrary factor for the sake of readability. In the inset, we plot the logarithm of $d \times \Phi_{\rm nl}(d)$, with d the distance to the *center* of the cylinder (same legend as on the main graph). This plot emphasizes the expected asymptotic behavior of the potential $\Phi_{\rm nl}(d) \sim \exp(-\kappa_{\rm D} d)/d$, with $d = \sqrt{r^2 + z^2}$. Curves have been also shifted by arbitrary factors.

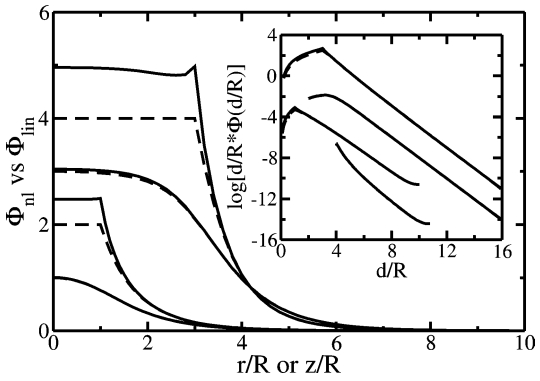

Fig. 7. Same as in Fig. 6 for $L/R = 6$, $\sigma = 10$, $\kappa_{\rm D} = 1.0$, $\Phi_{\rm eff} = 3.42$ on the axis $r = 0$, $r = R + \kappa_{\rm D}^{-1} = 2R$, $r = R + 5\kappa_{\rm D}^{-1} = 6R$, $z = 0$, $z = L/2 + \kappa_{\rm D}^{-1} = 4R$, and $z = L/2 + 5\kappa_{\rm D}^{-1} = 8R$. On the vertical axis, the curves have been multiplied by an arbitrary factor for the sake of readability. As in Fig. 6, the inset emphasizes the asymptotic decay of the potential, as $\Phi_{\rm nl}(d) \sim \exp(-\kappa_{\rm D} d)/d$, which is expected at large distances from the cylinder ($d = \sqrt{r^2 + z^2}$). Curves have been also shifted by arbitrary factors.

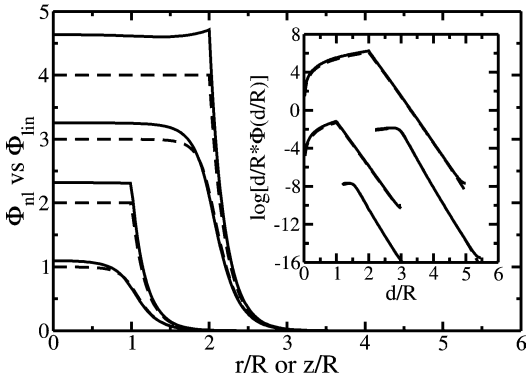

Fig. 8. Same as in Figs. 6 and 7 for $L/R = 4$, $\sigma = 10$, $\kappa_{\rm D} R = 5.0$, $\Phi_{\rm eff} = 1.41$ on the axis $r = 0$, $r = R + \kappa_{\rm D}^{-1} = 1.2R$, $r = R + 5\kappa_{\rm D}^{-1} = 2R$, $z = 0$, $z = L/2 + \kappa_{\rm D}^{-1} = 2.2R$, and $z = L/2 + 5\kappa_{\rm D}^{-1} = 3$.

the solution of the LPB equation (4) with a *fixed potential* boundary condition called the *effective surface potential*.

An agreement between these two solutions is expected to be valid in the saturation limit where the charge of the colloid is large [25]. We have therefore explored the parameter space (charge, aspect ratio) to test the validity of this prescription. In this paragraph, we show results in the region of the parameter space where an agreement is found. In other words, in the cases shown below, it is possible to fit the NLPB solution with a constant bare surface charge, with the LPB solution with a fixed potential boundary condition, using a single parameter fit: the effective surface potential Φ_0. Such a fit should only hold *for large distances* from the colloid (say, typically for distances larger than a few Debye length), for which the NLPB equation reduces to the LPB equation.

We shall precise in Section 3.4 the domain of validity, in parameter space, of the previous matching procedure. The results are presented in Figs. 6, 7, and 8.

It is important to emphasize that the agreement between these two solutions is not obvious *a priori*. Indeed for finite rod-like cylinders, the solution of the LPB (or NLPB) equations is quite different depending on the boundary condition under consideration: fixed surface charge, or fixed surface potential (at the colloid surface). This difference originates in particular in the so-called edge effects associated with the constant potential boundary condition. The fact that an agreement may be found between the NLPB with fixed charge and the LPB with fixed surface potential is therefore a non trivial point [25].

The insets of Figs. 6, 7, and 8 show that except in the immediate vicinity of the charged rods, NLPB and LPB solutions remarkably superimpose (the dashed lines are hardly distinguishable from the continuous ones). We conclude from figures Figs. 6, 7, and 8 that—at least in the conditions considered—a very good agreement can be found between the NLPB solution at fixed charge and the LPB solution at fixed potential.

3.3. Anisotropy of the electrostatic potential

We now focus on the anisotropy of the electrostatic potential at large distances. As emphasized in the previous curves, the potential decays as $\Phi_{\rm nl}(d) \sim \exp(-\kappa_{\rm D} d)/d$ in this limit, and one may extract an anisotropy factor $f(\theta)$, defined as

$$\Phi_{\rm nl}(d) = f[\theta] \frac{\ell_{\rm B}}{d} \exp(-\kappa_{\rm D} d), \tag{6}$$

which again is valid for large distances d from the center of the cylinder, $d = \sqrt{r^2 + z^2}$. For the cylinder shape colloid under consideration, the anisotropy factor depends only on the angle θ between the z axis and the direction (OM)

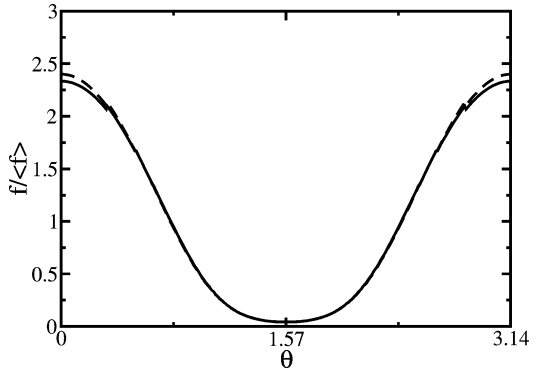

Fig. 9. Normalized anisotropic factor $f(\theta)/\langle f\rangle$ (for $L = 10$, $\sigma = 100$, $\kappa_D R = 1.0$). For any direction θ, f is computed from the asymptotic behavior of the potential, according to Eq. (6). Solid line: anisotropic factor computed from the solution, Φ_{nl}, of the nonlinear PB equation; dashed line: anisotropic factor computed from the solution of the linearized PB equation, Φ_{lin}, as obtained in Ref. [23].

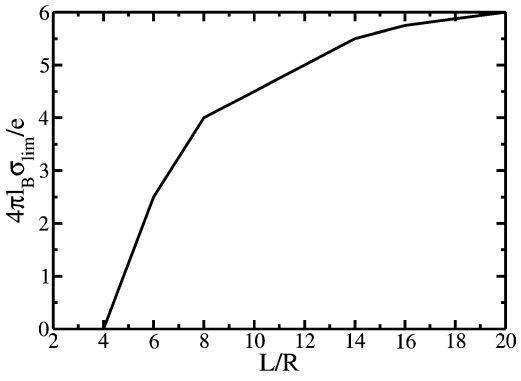

Fig. 10. Domain of validity of the constant potential prescription (see text) as a function of the dimensionless bare charge on the cylinder, and of the aspect ratio of the cylinder (here for $\kappa_D R = 1.0$). Above the $\sigma_{lim}(L)$ curve, the agreement between the exact solution Φ_{nl} of the nonlinear Poisson–Boltzmann equation for a cylinder carrying the bare charge σ_{bare} and the solution Φ_{lin} of the linearized equation for the same cylinder at a well-chosen fixed potential is better than 5% for distances larger than $r_0 = 4\kappa_D^{-1}$.

(O being the origin of the cylinder and M the point with coordinates $\{r, z\}$). This anisotropy factor is plotted in Fig. 9 as a function of θ (normalized by its average over the angles, $\langle f\rangle$). In this figure, we also compare this result with the anisotropy factor obtained at the level of the linearized PB equation with *fixed potential boundary condition* on the cylinder. The agreement is found to be very good, emphasizing again that the PB potential with fixed, large surface charge, does indeed match the LPB solution with a fixed potential on the cylinder for large distances from the colloid.

This figure reveals the strong anisotropy of the colloid, which, according to Eq. (6), persists at large distance from the colloid. In other words, the electrostatic potential, Eq. (6), never reduces to the spherical one at large distances, even for moderate anisotropy of the colloid.

3.4. Domain of validity of the constant potential prescription

We now consider the domain of validity of the previous prescription. More precisely, we have exhibited above examples showing that the LPB potential (with a fixed potential on the cylinder) may be matched to the PB solution with fixed large surface charge for large distances from the colloid.

According to results in different geometries (spheres and infinite cylinders) [25], such a prescription is actually expected for large bare charge on the colloid. However, one may also expect this prescription to be extended for all values of σ when the colloid anisotropy is weak (i.e., for low values of $\kappa_D L$ or aspects ratios L/R of order 1). Indeed, in these weak anisotropy cases, the geometry is quite close to that of a sphere, for which, by construction, the general solution of the LPB (NLPB) equations are identical for constant surface charge and constant surface potential. In this limit, it is therefore always possible to define a surface potential such that a matching between these two solutions is found.

In Fig. 10, we gather results emerging from the previous matching procedure and represent the domain of validity of the previous constant effective surface potential prescription, as a function of the aspect ratio L/R (for a given Debye length). We have somewhat arbitrarily defined domain of validity of the previous prescription, as the region for which the two solutions Φ_{nl} and Φ_{lin} differ by less than 5% for all distances larger than a minimum distance r_0, here chosen as $r_0 = 4\ell_D$ (with ℓ_D the Debye length). One finds that such a requirement is reached for sufficiently large surface charges, allowing to define a minimum surface charge on the colloid σ_{lim} above which the constant potential prescription holds. In the regime of aspect ratio around unity ($2 < L/R < 4$), the constant potential prescription appears to be always valid according to the chosen criterion. This reflects the fact discussed above that for intermediate aspect ratio $L/R \sim 2$, the geometry is close to a spherical geometry, for which one may always define a potential such that the PB and LPB solutions matches at large distances. This is clearly not the case for intermediate geometries with larger aspect ratios. However a constant potential prescription at the LPB level is recovered for sufficiently large bare surface charge on the colloid, as emphasized by the existence of a minimum charge σ_{lim}.

Note that in the present study, we only focused on cylinders with aspect ratio larger than one (in practice $L/R > 2$). One expects similar results to hold in the disk case $L/R < 1$, with the existence of a minimum surface charge above which the constant potential holds (especially in the strong anisotropy limit, $L/R \ll 1$).

Figs. 6, 7, and 8 show that the matching of Φ_{nl} by Φ_{lin} on the symmetry axis of the cylinder $r = 0$ and plane $z = 0$ is valid as soon as the distance from the surface of the colloid is larger than κ_D^{-1} (at least for $\kappa_D R = 0.2$ and $\kappa_D R = 1.0$), which is a much less restrictive condition than the arbitrary one chosen for defining σ_{lim} in Fig. 10. For the sake of simplicity, we shall keep in mind that the matching procedure remains essentially valid at one Debye length of the colloid if our strong criterion is fulfilled but may break down for

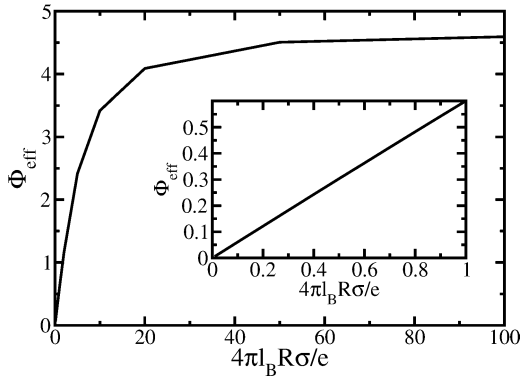

Fig. 11. Dependence of the effective surface potential Φ_{eff} as a function of the (dimensionless) bare charge on the cylinder $4\pi\ell_B R\sigma_{\text{bare}}/e$ for $L/R = 4$ and $\kappa_D = 1.0$. The inset is a zoom into the weak coupling region.

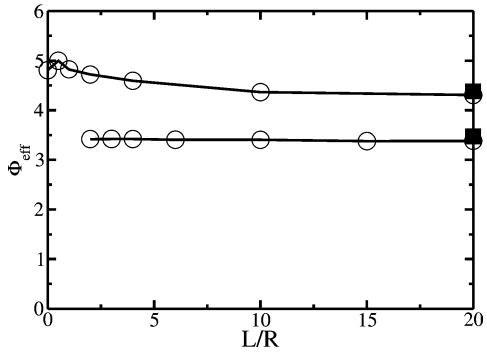

Fig. 12. Dependence of the effective surface potential Φ_{eff} as a function of the aspect ratio of the cylinder L/R, for $\sigma_{\text{bare}} = 10$ and $\sigma_{\text{bare}} = 100$ (solid lines from bottom to top). The Debye screening factor is $\kappa_D R = 1.0$. Open symbols represent the computed values of the effective surface potential and filled squares indicate the values of Φ_{eff} for an infinite cylinder.

particular regions (e.g., close to the edges) between ℓ_D and $4\ell_D$ depending on the parameters of the problem (σ, $\kappa_D R$, and L).

3.5. *Effective "linear" surface potential*

We consider here the value of the effective surface potential of the colloid, Φ_{eff}, found by the previous matching procedure. As shown in Fig. 11, Φ_{eff} increases with the value of σ_{bare}. Moreover, for large values of σ_{bare}, the saturation regime is reached and the effective surface potential becomes independent of the bare charge σ_{bare}, as for infinite cylinders [25]. We recover the result obtained in [25], that in the saturation regime, the effective potential of the polyelectrolyte is of the order of a few $k_B T/e$.

This saturation regime originates in the accumulation of counterions in the region very close to the colloid surface as the bare charge of the cylinder increases. This nonlinear "condensation" of counterions results in an effective surface potential which is independent of the bare charge.

We now turn to the influence of the aspect ratio of the cylinder on the effective surface potential. As shown in Fig. 12, this dependence is found to be quite weak. Moreover, as expected the value for large aspect ratio L/R reduces to that of the infinite cylinder (as obtained numerically following the method put forward in [31]).

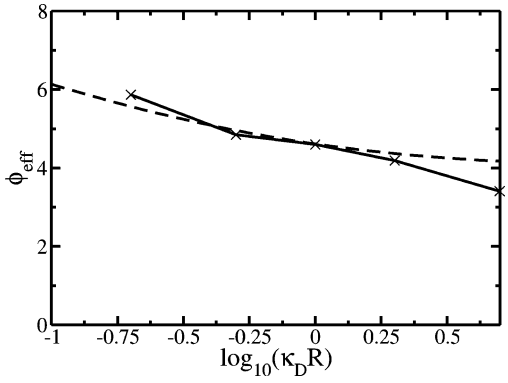

Fig. 13. Dependence of the effective surface potential Φ_{eff} as a function of the Debye screening factor $\kappa_D R$. The aspect ratio of the cylinder is here $L/R = 4$ and the bare charge is $\sigma_{\text{bare}} = 100$. The dashed line represents the value of the effective surface potential for infinite cylinders, in the saturation limit, as obtained numerically following the method of Ref. [31].

Let us now analyze the influence of the salt concentration (see Fig. 13). A few remarks may be drawn from this figure. First, as expected, the effective surface potential goes toward a value close to $\Phi_{\text{eff}} = 4$ for large screening factors. This is because in this limit curvature effects no longer play a role and the potential reduces to the planar result $\Phi_{\text{eff}} = 4$ [25]. Second, it is interesting to note that the values for Φ_{eff} are close to those obtained for infinite cylinders in the saturation limit (see the dashed line in Fig. 13), even if the aspect ratio is quite low in the present case.

We conclude this section by providing a table of the effective surface potential Φ_{eff} for several values of the parameters of the cylinder. Since Fig. 12 shows that Φ_{eff} does not much depend on the length L of the rod, we only report the asymptotic value for large L/R values. In this table, the effective surface potential Φ_{eff} is reported for given values of the bare surface charge $\sigma_{\text{adim}} = 4\pi\ell_B R\sigma/e$ and Debye length $\kappa_D R$:

$\kappa_D R \vert\vert \sigma_{\text{adim}}$	1	2	5	10	20	50	100
0.2	1.19	2.28	4.40	5.41	5.70	5.82	5.87
0.5	0.867	1.66	3.24	4.25	4.65	4.77	4.85
1.0	0.601	1.16	2.42	3.42	4.08	4.50	4.59
2.0	0.375	0.737	1.65	2.60	3.40	3.99	4.19
5.0	0.161	0.322	0.777	1.41	2.19	3.04	3.44

This table makes it possible to compute the interaction energy $U_{12}(r)$ between two rodlike macromolecules for given values of $\sigma_{\text{adim}} = 4\pi\ell_B R\sigma_{\text{bare}}/e$ and $\kappa_D R$. The expression for the interaction energy for two rodlike macromolecules has been obtained in Ref. [23] and recalled in Appendix C. By replacing Φ_0 with the value provided by this table in Eq. (C.2) of Appendix C, one deduces an explicit expression for the interaction energy at large distances, using Eq. (C.1).

4. Conclusion

In this paper, we have solved numerically the *nonlinear* Poisson–Boltzmann (NLPB) equation for rodlike polyelectrolytes with finite aspect ratios and compared the results to the solution of the *linearized* Poisson–Boltzmann (LPB) equation. This led us to the conclusion that the NLPB solution with a fixed bare charge for the electrostatic potential coincides with the LPB one at large distances from the colloid, provided an *effective boundary condition* of *fixed potential* is applied in the LPB approach. This generalizes therefore the results obtained for spheres and infinite cylinders [25], to polyelectrolytes with a finite anisotropy. The *effective surface potential* is found to be only weakly dependent on the aspect ratio of the cylinder and Debye screening factor $\kappa_D R$. When the bare charge of the colloid becomes large, this effective surface potential reaches a saturation value fixed by the balance between electrostatic and entropic effects, i.e., of the order of a few $k_B T/e$. We provide an easy-to-use table to compute the interaction energy of two finite charged rods for given values of its bare surface charge $4\pi\ell_B\sigma_{bare}/e$ and of the Debye length of the ionic solution $\kappa_D R$.

The present work shows that the far-field interaction between two highly charged anisotropic colloids can be accounted for at the level of the LPB description with a fixed effective surface potential. This problem has been considered in Ref. [23], providing a generalized anisotropic DLVO interaction, in the form

$$U_{12}(r) \sim f_1(\mathbf{u}_1) f_2(\mathbf{u}_2) \frac{e^{-\kappa_D r}}{4\pi\epsilon r}, \tag{7}$$

where $f_i(\mathbf{u}_i)$ characterizes the anisotropy of the interaction ($\mathbf{u}_i$ denoting a vector defining the orientation of the colloid) and depends on the specific geometry of the colloid under consideration. This anisotropy factor does moreover take into account the charge accumulation in the vicinity of the edges of the colloid (the so-called edge effect). We refer to Ref. [23] for further details on these aspects.

The next step of this study consists in analyzing the consequences of this anisotropic interaction on the phase behavior of highly charged rodlike macromolecules. Work along these lines is in progress.

Appendix A. The iterative procedure followed

The NLPB equation (2) can formally be written as

$$(-\Delta+\kappa^2)\Phi(\mathbf{r}) = \rho_{cyl}(\mathbf{r}) + \left[\kappa^2\Phi(\mathbf{r}) - \kappa_D^2(\mathbf{r})\sinh\Phi(\mathbf{r})\right], \tag{A.1}$$

where $\rho_{cyl}(\mathbf{r})$ is the bulk charge density carried by the cylinder (here, a surface charge density), $\kappa_D(\mathbf{r})$ the inverse of the Debye length in $\mathbf{r}$ (equal to 0 inside $\mathcal{C}$ and κ_D outside) and κ an arbitrary constant which will be chosen equal to κ_D to make the term between brackets vanish far from $\mathcal{C}$. Introducing the Green function $G_\kappa(\mathbf{r},\mathbf{r}')$ associated with the linear operator $(-\Delta+\kappa^2)$,

$$\forall \mathbf{r},\mathbf{r}' \in \mathrm{WS}, \quad (-\Delta_{\mathbf{r}}+\kappa^2)G_\kappa(\mathbf{r},\mathbf{r}') = \delta(\mathbf{r}-\mathbf{r}'),$$

one may invert Eq. (A.1) as

$$\begin{aligned}\Phi(\mathbf{r}) &= F[\Phi](\mathbf{r}) \\ &= \iiint_{\mathrm{WS}} G_\kappa(\mathbf{r},\mathbf{r}')\,\mathbf{dr}'\left\{\rho_{cyl}(\mathbf{r}')\right. \\ &\quad \left. + \left[\kappa^2\Phi(\mathbf{r}') - \kappa_D^2(\mathbf{r}')\sinh\Phi(\mathbf{r}')\right]\right\}.\end{aligned} \tag{A.2}$$

Note that in the case of the WS cell model, $G_\kappa(\mathbf{r},\mathbf{r}')$ may be chosen to obey the boundary conditions

$$\forall \mathbf{r}\in\mathcal{S},\ \forall \mathbf{r}'\in\mathrm{WS}, \quad \mathbf{grad}_{\mathbf{r}} G_\kappa(\mathbf{r},\mathbf{r}')\cdot\mathbf{n}(\mathbf{r}) = 0.$$

It was shown that in this case that the required Green's function can be expressed in the form of the Bessel–Dini series [30]

$$G_\kappa(\mathbf{r},\mathbf{r}') = \sum_{n=0}^{\infty} \mathcal{C}_n^{\pm}(\mathbf{r}') J_0\left(y_n \frac{r}{R_{WS}}\right)\cosh\left(\frac{h_{WS}\mp z}{\Lambda_n}\right), \tag{A.3}$$

where (r,z) are the usual cylindrical coordinates (without the polar angle φ because of the symmetry of revolution around the axis of $\mathcal{C}$), the signs $+$ and $-$ correspond to the situations $z>z'$ and $z<z'$, respectively, y_n is the nth root the Bessel function J_1 (with the convention $y_0=0$) and $\Lambda_n^2 = R_{WS}^2/(y_n^2+\kappa^2 R_{WS}^2)$. The coefficients $\mathcal{C}_n^{\pm}(\mathbf{r}')$ are given by

$$\mathcal{C}_n^{\pm}(\mathbf{r}') = \frac{2\Lambda_n R}{R_{WS}^2\sinh\left(\frac{2h_{WS}}{\Lambda_n}\right)} \frac{J_0\left(y_n\frac{r'}{R_{WS}}\right)}{J_0^2(y_n)}\cosh\left(\frac{h_{WS}\pm z'}{\Lambda_n}\right).$$

In order to solve the self-consistent equation (A.2) numerically, we divide the WS cell in subcells $\mathcal{C}_i$. As shown in Fig. 1, the WS cell of radius R_{WS} and height $2h_{WS}$ is divided in $N_{R_{WS}} \times N_{h_{WS}}$ cylindrical rings $\mathcal{C}_i$ of radii $R_{WS} i/N_{R_{WS}}$ (where i is a positive integer less than $N_{R_{WS}}$, of width $R_{WS}/N_{R_{WS}}$ and of height $2h_{WS}/N_{h_{WS}}$, which are represented with dotted lines. Each of these cells, except the ones located in the vicinity of the boundary of the WS cell, are centered on the nodes $\mathbf{r}_i$ of the lattice represented with dashed lines where we compute Φ_{nl}.

Equation (A.2) is accordingly discretized on the subcells. The first source term on the r.h.s. can be re-expressed in terms of the surface charge density σ,

$$\iiint_{\mathrm{WS}} G_\kappa(\mathbf{r},\mathbf{r}')\rho_{cyl}(\mathbf{r}')\,\mathbf{dr}' = \sigma\int_{\Sigma} G_\kappa(\mathbf{r},\mathbf{r}')\,\mathrm{d}S', \tag{A.4}$$

whose explicit expression is given in Appendix B. The second term on the r.h.s. of Eq. (A.2), which generically takes the form

$$I[f] = \iiint_{\mathrm{WS}} G_\kappa(\mathbf{r},\mathbf{r}')f(\mathbf{r}')\,\mathbf{dr}', \tag{A.5}$$

with f a smooth function of $\mathbf{r}'$, is discretized according to

$$I[f] = \sum_{\mathbf{r}'_i \in \mathcal{C}_i} f(\mathbf{r}'_i) \iiint_{\mathcal{C}_i} G_\kappa(\mathbf{r}, \mathbf{r}'_i)\, \mathbf{dr}', \tag{A.6}$$

where the integrals on the Green function G_κ are explicitly computed in order to avoid numerical divergences.

The discretized self-consistent equation (A.2) is solved using an iterative procedure: after each step i, a new potential $\Phi_{i+1}(\mathbf{r})$ is computed through

$$\Phi_{i+1}(\mathbf{r}) = \alpha \Phi_i(\mathbf{r}) + (1-\alpha) F[\Phi_i](\mathbf{r}), \tag{A.7}$$

where α is a mixing parameter ($\alpha \sim 0.9$). The potential Φ_{nl} is initialized at the first step with the solution of the LPB equation, Φ_{lin}, created by the same object but with a given surface potential boundary condition (namely, $\Phi = 4$ on the surface). The iterations are stopped when the greatest value of $(\Phi_{i+1}(\mathbf{r}) - \Phi_i(\mathbf{r}))/\Phi_i(\mathbf{r})$ is smaller than 10^{-4} for all the points $\mathbf{r}$ of the WS cell. For example, the calculation of Φ_{nl} for $\kappa_{\mathrm{D}} R = 1.0$, $L = 4R$, $\sigma = 10$ with a 100×200 points lattice starting with Φ_{nl} can be achieved in approximately 100 iterations.

Typical values of the parameters are, in the case of infinite dilution, $R_{\mathrm{WS}} = 10\ell_{\mathrm{D}}$ and $h_{\mathrm{WS}} - L/2 \simeq 10\ell_{\mathrm{D}}$, $N_{R_{\mathrm{WS}}} = 100$ or 200, $N_{h_{\mathrm{WS}}} = 200$ or 400 and the sums over n are truncated after 1500 Bessel–Dini modes.

Appendix B. Expression of the Green functions for the numerical resolution of NLPB

The source term $\iiint G(\mathbf{r}, \mathbf{r}')\rho_{\mathrm{cyl}}(\mathbf{r}')\, \mathbf{dr}'$ can be written as

$$\sigma \int G(\mathbf{r}, \mathbf{r}')\, \mathrm{d}S'.$$

Straightforward but lengthy calculations lead to

- If $|z| \leqslant L/2$

$$\begin{aligned}
&\iiint G(\mathbf{r}, \mathbf{r}')\rho_{\mathrm{cyl}}(\mathbf{r}')\, \mathbf{dr}' \\
&\quad = G_{\text{full infinite cyl}}(R, r) \\
&\qquad - \sum_{n=0}^{\infty} \frac{\sigma \Lambda_n^2}{R_{\mathrm{WS}}^2} \frac{J_0\big(y_n \frac{R}{R_{\mathrm{WS}}}\big) J_0\big(y_n \frac{r}{R_{\mathrm{WS}}}\big)}{J_0^2(y_n)} \\
&\qquad \times \left\{ \frac{\exp\big(-\frac{L/2-|z|}{\Lambda_n}\big) - \exp\big[-\frac{2h_{\mathrm{WS}}-(L/2-|z|)}{\Lambda_n}\big]}{1-\exp\big(-\frac{2h_{\mathrm{WS}}}{\Lambda_n}\big)} \right. \\
&\qquad \left. + \frac{\exp\big(-\frac{L/2+|z|}{\Lambda_n}\big) - \exp\big[-\frac{2h_{\mathrm{WS}}-(L/2+|z|)}{\Lambda_n}\big]}{1-\exp\big(-\frac{2h_{\mathrm{WS}}}{\Lambda_n}\big)} \right\} \\
&\qquad + \sum_{n=0}^{\infty} \frac{\sigma \Lambda_n}{y_n R_{\mathrm{WS}}} \frac{J_1\big(y_n \frac{R}{R_{\mathrm{WS}}}\big) J_0\big(y_n \frac{r}{R_{\mathrm{WS}}}\big)}{J_0^2(y_n)} \\
&\qquad \times \left\{ \frac{\exp\big(-\frac{L/2-|z|}{\Lambda_n}\big) + \exp\big[-\frac{2h_{\mathrm{WS}}-(L/2-|z|)}{\Lambda_n}\big]}{1-\exp\big(-\frac{2h_{\mathrm{WS}}}{\Lambda_n}\big)} \right. \\
&\qquad \left. + \frac{\exp\big(-\frac{L/2+|z|}{\Lambda_n}\big) + \exp\big[-\frac{2h_{\mathrm{WS}}-(L/2+|z|)}{\Lambda_n}\big]}{1-\exp\big(-\frac{2h_{\mathrm{WS}}}{\Lambda_n}\big)} \right\},
\end{aligned}$$

where $G_{\text{full infinite cyl}}(R, r)$ is the electrostatic potential calculated in a WS cell of radius R_{WS} of an infinite cylinder of radius R immersed in an electrolyte with Debye length ℓ_{D} (the electrolyte filling the interior of the cylinder) and carrying a uniform surface charge density σ. The expression of $G_{\text{full infinite cyl}}(R, r)$ is written

– if $r \leqslant R$

$$\begin{aligned}
&G_{\text{full infinite cyl}}(R, r) \\
&\quad = \sigma \left[K_0(\kappa_{\mathrm{D}} R) + \frac{K_1(\kappa_{\mathrm{D}} R_{\mathrm{WS}}) I_0(\kappa_{\mathrm{D}} R)}{I_1(\kappa_{\mathrm{D}} R_{\mathrm{WS}})} \right] I_0(\kappa_{\mathrm{D}} r);
\end{aligned}$$

– if $r \geqslant R$

$$\begin{aligned}
&G_{\text{full infinite cyl}}(R, r) \\
&\quad = \sigma I_0(\kappa_{\mathrm{D}} R) K_0(\kappa_{\mathrm{D}} r) \\
&\qquad + \sigma \left[K_0(\kappa_{\mathrm{D}} R) + \frac{K_1(\kappa_{\mathrm{D}} R_{\mathrm{WS}}) I_0(\kappa_{\mathrm{D}} R)}{I_1(\kappa_{\mathrm{D}} R_{\mathrm{WS}})} \right] \\
&\qquad \times I_0(\kappa_{\mathrm{D}} r).
\end{aligned}$$

- If $z = L/2$

$$\begin{aligned}
&\iiint G(\mathbf{r}, \mathbf{r}')\rho_{\mathrm{cyl}}(\mathbf{r}')\, \mathbf{dr}' \\
&\quad = \frac{G_{\text{infinite cyl}}(R, r)}{2} \\
&\qquad - \sum_{n=0}^{\infty} \frac{\sigma \Lambda_n^2}{R_{\mathrm{WS}}^2} \frac{J_0\big(y_n \frac{R}{R_{\mathrm{WS}}}\big) J_0\big(y_n \frac{r}{R_{\mathrm{WS}}}\big)}{J_0^2(y_n)} \\
&\qquad \times \frac{\exp\big(-\frac{L}{\Lambda_n}\big) - \exp\big(-\frac{2h_{\mathrm{WS}}-L}{\Lambda_n}\big)}{1-\exp\big(-\frac{2h_{\mathrm{WS}}}{\Lambda_n}\big)} \\
&\qquad + \Phi_{\mathrm{disk}}(R, r, 0) \\
&\qquad + \sum_{n=0}^{\infty} \frac{\sigma \Lambda_n}{y_n R_{\mathrm{WS}}} \frac{J_1\big(y_n \frac{R}{R_{\mathrm{WS}}}\big) J_0\big(y_n \frac{r}{R_{\mathrm{WS}}}\big)}{J_0^2(y_n)} \\
&\qquad \times \frac{\exp\big(-\frac{L}{\Lambda_n}\big) + \exp\big(-\frac{2h_{\mathrm{WS}}-L}{\Lambda_n}\big)}{1-\exp\big(-\frac{2h_{\mathrm{WS}}}{\Lambda_n}\big)},
\end{aligned}$$

where the expression of $G_{\mathrm{disk}}(R, r, 0)$ is

$$G_{\mathrm{disk}}(R, r, 0) = \frac{1}{2} \int_0^{\infty} \frac{J_1(\kappa_{\mathrm{D}} R u) J_0(\kappa_{\mathrm{D}} r u)\, \mathrm{d}u}{\sqrt{u^2 + \kappa_{\mathrm{D}}^2 R^2}}.$$

- If $|z| > L/2$

$$\begin{aligned}
&\iiint G(\mathbf{r}, \mathbf{r}')\rho_{\mathrm{cyl}}(\mathbf{r}')\, \mathbf{dr}' \\
&\quad = \sum_{n=0}^{\infty} \frac{\sigma \Lambda_n^2}{R_{\mathrm{WS}}^2} \frac{J_0\big(y_n \frac{R}{R_{\mathrm{WS}}}\big) J_0\big(y_n \frac{r}{R_{\mathrm{WS}}}\big)}{J_0^2(y_n)} \\
&\qquad \times \left\{ \frac{\exp\big(-\frac{|z|-L/2}{\Lambda_n}\big) - \exp\big(-\frac{|z|+L/2}{\Lambda_n}\big)}{1-\exp\big(-\frac{2h_{\mathrm{WS}}}{\Lambda_n}\big)} \right.
\end{aligned}$$

$$+\frac{\exp\left[-\frac{2h_{\mathrm{WS}}-(|z|+L/2)}{\Lambda_n}\right]-\exp\left[-\frac{2h_{\mathrm{WS}}-(|z|-L/2)}{\Lambda_n}\right]}{1-\exp\left(-\frac{2h_{\mathrm{WS}}}{\Lambda_n}\right)}\Bigg\}$$
$$+\sum_{n=0}^{\infty}\frac{\sigma\Lambda_n}{y_n R_{\mathrm{WS}}}\frac{J_1\left(y_n\frac{R}{R_{\mathrm{WS}}}\right)J_0\left(y_n\frac{r}{R_{\mathrm{WS}}}\right)}{J_0^2(y_n)}$$
$$\times\Bigg\{\frac{\exp\left(-\frac{|z|-L/2}{\Lambda_n}\right)+\exp\left[-\frac{2h_{\mathrm{WS}}-(|z|-L/2)}{\Lambda_n}\right]}{1-\exp\left(-\frac{2h_{\mathrm{WS}}}{\Lambda_n}\right)}$$
$$+\frac{\exp\left(-\frac{|z|+L/2}{\Lambda_n}\right)+\exp\left[-\frac{2h_{\mathrm{WS}}-(|z|+L/2)}{\Lambda_n}\right]}{1-\exp\left(-\frac{2h_{\mathrm{WS}}}{\Lambda_n}\right)}\Bigg\}.$$

Appendix C. Approximate generalized DLVO expression of the interaction potential between cylinders

In Ref. [23], we have obtained the electrostatic interaction energy between two anisotropic macromolecules, which writes

$$U_{12}(r)=\frac{\tilde{Z}_1\tilde{Z}_2\ell_{\mathrm{B}}f_1(\mathbf{u}_1)f_2(\mathbf{u}_2)e^{-\kappa_{\mathrm{D}}r}}{r}. \tag{C.1}$$

Simple approximate expressions for the anisotropic factor $f(\vec{u})$ have been obtained for a finite-size cylinder of length L and radius R at fixed potential Φ_0, in the form [23]

$$f(\vec{u})=\frac{\tilde{Z}_{\mathrm{cyl}}}{\tilde{Z}}f_{\mathrm{cyl}}(\theta)+\frac{\tilde{Z}_{\mathrm{head}}}{\tilde{Z}}f_{\mathrm{head}}(\theta), \tag{C.2}$$

with θ the angle between the main axis of the cylinder and the direction OM (M being the point under consideration and O the center of the cylinder).

In the above expression, the auxiliary charges $\tilde{Z}_{\mathrm{cyl}}$, $\tilde{Z}_{\mathrm{head}}$, and $\tilde{Z}$, as well as the anisotropy factors $f_{\mathrm{cyl}}(\theta)$ and $f_{\mathrm{head}}(\theta)$ are given by

$$\tilde{Z}_{\mathrm{cyl}}\frac{\ell_{\mathrm{B}}}{R}=\frac{1}{2}\frac{L}{R}\Phi_0\frac{1}{I_0(\kappa_{\mathrm{D}}R)K_0(\kappa_{\mathrm{D}}R)},$$
$$\tilde{Z}_{\mathrm{head}}\frac{\ell_{\mathrm{B}}}{R}=\frac{\kappa_{\mathrm{D}}R\Phi_0}{1-e^{-\kappa_{\mathrm{D}}R}}\left[1-\frac{1}{2I_0(\kappa_{\mathrm{D}}R)}\right],$$
$$\tilde{Z}=\tilde{Z}_{\mathrm{cyl}}+\tilde{Z}_{\mathrm{head}}$$

and

$$f_{\mathrm{cyl}}(\theta)=I_0(\kappa_{\mathrm{D}}R\sin\theta)\frac{\sinh\left(\frac{\kappa_{\mathrm{D}}L\cos\theta}{2}\right)}{\left(\frac{\kappa_{\mathrm{D}}L\cos\theta}{2}\right)},$$
$$f_{\mathrm{head}}(\theta)=\frac{2I_1(\kappa_{\mathrm{D}}R\sin\theta)}{\kappa_{\mathrm{D}}r_0\sin\theta}\cosh\left(\frac{\kappa_{\mathrm{D}}L\cos\theta}{2}\right).$$

References

[1] I. Langmuir, J. Chem. Phys. 6 (1938) 873.
[2] H. Zocher, Z. Anorg. Chem. 147 (1925) 91.
[3] D. van der Beek, H.N.W. Lekkerkerker, Europhys. Lett. 61 (2003) 702.
[4] O. Pelletier, P. Davidson, C. Bourgaux, J. Livage, Europhys. Lett. 48 (1999) 53.
[5] S. Fraden, G. Maret, D.L.D. Caspar, R.B. Meyer, Phys. Rev. Lett. 63 (1989) 2068.
[6] B. Guilleaume, J. Blaul, M. Ballauff, M. Witteman, M. Rehahn, G. Goerigk, Eur. Phys. J. E 8 (2002) 299.
[7] H. von Berlepsch, C. Bettcher, A. Ouart, S. Duehne, S. Kirstein, J. Phys. Chem. B 104 (2000) 5255.
[8] J.-C.P. Gabriel, F. Camerel, B.J. Lemaire, H. Desvaux, P. Davidson, P. Batail, Nature 413 (2001) 504.
[9] L. Onsager, Ann. N.Y. Acad. Sci. 51 (1949) 627.
[10] E.J.W. Verwey, J.T.G. Overbeek, Theory of the Stability of Lyophobic Colloids, Elsevier, Amsterdam, 1948.
[11] K.R. Purdy, Z. Dogic, S. Fraden, A. Rühm, L. Lurio, S.G.J. Mochrie, Phys. Rev. E 67 (2003) 031708.
[12] A. Stroobants, H.N.W. Lekkerkerker, T. Odijk, Macromolecules 19 (1986) 2232.
[13] S.-L. Lee, J. Chem. Phys. 87 (1987) 4972.
[14] B.J. Lemaire, P. Davidson, J. Ferre, J.-P. Jamet, P. Panine, I. Dozov, J.-P. Jolivet, Phys. Rev. Lett. 88 (2002) 125507.
[15] E.M. Kramer, J. Herzfeld, Phys. Rev. E 61 (2000) 6872.
[16] A. Mourchid, A. Delville, J. Lambard, E. Lécolier, P. Levitz, Langmuir 11 (1995) 1942.
[17] J.-C.P. Gabriel, C. Sanchez, P. Davidson, J. Phys. Chem. 100 (1996) 11,139.
[18] A. Mourchid, E. Lécolier, H. van Damme, P. Levitz, Langmuir 14 (1998) 4718.
[19] D. Bonn, H. Kellay, H. Tanaka, G. Wedgam, J. Meunier, Langmuir 15 (1999) 7534.
[20] D. Bonn, H. Tanaka, G. Wedgam, H. Kellay, J. Meunier, Europhys. Lett. 45 (1999) 52.
[21] P. Levitz, E. Lécolier, A. Mourchid, A. Delville, S. Lyonnard, Europhys. Lett. 49 (2000) 672.
[22] T. Nicolai, S. Cocard, Eur. Phys. J. E 5 (2001) 227.
[23] D. Chapot, L. Bocquet, E. Trizac, J. Chem. Phys. 120 (2004) 3969.
[24] E. Trizac, L. Bocquet, R. Agra, J.-J. Weis, M. Aubouy, J. Phys. Condens. Matter 14 (2002) 9339.
[25] L. Bocquet, E. Trizac, M. Aubouy, J. Chem. Phys. 117 (2002) 8138; E. Trizac, L. Bocquet, M. Aubouy, Phys. Rev. Lett. 89 (2002) 248,301.
[26] A. Mourchid, A. Delville, J. Lambard, E. Lécolier, P. Levitz, Langmuir 11 (1995) 1942.
[27] D. Bonn, H. Kellay, H. Tanaka, G. Wedgam, J. Meunier, Langmuir 15 (1999) 7534.
[28] R. Agra, F. van Wijland, E. Trizac, Phys. Rev. Lett., in press.
[29] In practice, $\kappa a > 1$ is sufficient.
[30] R.J.F. Leote de Carvalho, E. Trizac, J.P. Hansen, Phys. Rev. E 61 (2000) 1634.
[31] E. Trizac, L. Bocquet, M. Aubouy, H.H. von Grünberg, Langmuir 19 (2003) 4027.